photonics

MDPI

Article

Near-Infrared Absorption Enhancement of GaAs Photocathode Through "Sandwich" Micro-Nano Structure

Ziyang Xiao [1,2], Miao Dong [1,3], Yonggang Huang [1,3,4,*], Jinhui Yang [1,3], Peng Jiao [1,3], Pan Shi [1,5], Yajie Du [1,3], Ying He [6], Jing Cheng [1,2] and Yinsheng Xu [2,*]

1 China Building Materials Academy, Beijing 100024, China
2 State Key Laboratory of Silicate Materials for Architectures, Wuhan University of Technology, Wuhan 430070, China
3 Key Laboratory of Special Optoelectronic Glass in Building Materials Industry, China Building Materials Academy, Beijing 100024, China
4 Glass-Based Functional Material Technology Innovation Center, China Building Materials Academy, Beijing 100024, China
5 China National Building Material Guangxin Technology Co., Ltd., Zaozhuang 277101, China
6 College of General Education, Xi'an Mingde Institute of Technology, Xi'an 710124, China
* Correspondence: huangyonggang@cbma.com.cn (Y.H.); xuyinsheng@whut.edu.cn (Y.X.)

Abstract

In this paper, a nano-layered transmission GaAs photocathode structure is proposed. The near-infrared absorption of the photocathode is enhanced by inserting a "sandwich" structure of nano-SiO_2 layer + Si_3N_4 nanopillar array + nano-SiO_2 layer between the cathode optical window and the photocathode. Compared with the flat film structure GaAs photocathode used in the current third-generations image intensifiers, the optical absorption of the optimized "sandwich" structure GaAs photocathode in the near-infrared band has been significantly improved: when the wavelength λ is 868 nm and 896 nm, the optical absorption is increased by 41.69%, 55.08%, respectively. The effects of structural parameters including film thickness and grating filling medium on the light absorption of photocathode are investigated. The results show that the near-infrared light absorption enhancement is the most obvious when Si_3N_4 is selected as the grating filling medium for the current design, and the deposition of SiO_2 film with 10 nm thickness could effectively prevent the damage of Si_3N_4 during bonding with the photocathode. The theoretical analyses offer important guidance in material selection and structural optimization in the grating cathode optical window used in the third-generation image intensifier for improving performance.

Keywords: nanopillar array; GaAs photocathode; guided-mode resonance; optical performance

Check for updates

Received: 22 November 2025
Revised: 29 December 2025
Accepted: 14 January 2026
Published: 16 January 2026

Copyright: © 2026 by the authors. Licensee MDPI, Basel, Switzerland. This article is an open access article distributed under the terms and conditions of the Creative Commons Attribution (CC BY) license.

1. Introduction

Gallium arsenide negative electron affinity (NEA) photocathodes are the core photoelectric conversion components of third-generation image intensifiers. They enable efficient photoelectron excitation and emission, featuring high quantum efficiency (QE), low dark emission, narrow energy and angular distributions of emitted electrons, long-wavelength tunability, and great potential for wavelength response extension. Owing to these advantages, they are widely applied in spin-polarized electron sources, photodetectors, and low-light-level imaging systems [1–5]. In application scenarios of low-light-level night vision devices, photocathodes typically detect the reflected light of a scene. Taking grassland

as a typical example, the reflected spectral energy of night-sky illumination is generally weak in the visible band but concentrated in the near-infrared region [6]. For conventional planar GaAs photocathodes, the intrinsic absorption coefficient and thickness limitations cause a rapid decrease in absorption efficiency in the long-wavelength region, resulting in significantly reduced quantum efficiency. This severely restricts the near-infrared detection capability of photoelectric imaging systems under extremely low illumination.

According to Spicer's three-step model of photoemission [7], increasing the absorption of incident photons, enhancing photoelectron transport, and reducing the electron emission work function are three main approaches to improving photocathode quantum efficiency. Graded-doping or graded-bandgap structures [8–11] bend the energy bands and form internal built-in electric fields. These built-in fields facilitate electron transport toward the emitting surface, increasing their diffusion length and enhancing the spectral response of the photocathode. Chen et al. [2] grew a transmission-mode (t-mode) AlGaAs photocathode with a graded Al-composition structure using molecular beam epitaxy (MBE). When the outermost GaAs layer reached nano-scale, the quantum efficiency in the blue-green spectral region increased significantly. This is because nano-scale surface structures exhibit quantum confinement effects, which reduce the surface electron affinity and enhance the electron escape probability, thereby allowing more photoelectrons to be emitted into the vacuum. Enhancing optical absorption is also a common method for improving quantum efficiency. Typical structures include distributed Bragg reflector (DBR) structures and nano-array structures. Wang et al. [12] utilized a DBR to reflect specific wavelengths of transmitted light back into the emission layer to further enhance absorption, thereby improving the response of AlGaAs photocathodes at 532 nm. For t-mode multi-alkali photocathodes used in super-second-generation image intensifiers, a transmissive diffraction grating on the glass window to increase the optical path within the emission layer was proposed [13]. It is reported that the visible light and near-infrared light absorption is effectively enhanced without altering the photocathode thickness. With regard to negative electron affinity (NEA) GaAs photocathodes, existing studies indicate that, for both reflection-mode (r-mode) [14–16] and transmission-mode photocathodes [17], the prevailing approach is to nanostructure one of the photocathode layers. By contrast, design strategies that do not modify the intrinsic photocathode structure, similar to those adopted in super-second-generation image intensifiers, have only been reported for nano-scale NEA photocathodes [18].

In this work, a "sandwich" t-mode NEA GaAs photocathode structure consisting of a nano-SiO_2 layer, a Si_3N_4 nanopillar array (NPA), and another nano-SiO_2 layer inserted between the photocathode window was proposed. This configuration aims to enhance near-infrared (800–900 nm) absorption in GaAs photocathode. An optical model based on the finite-difference time-domain (FDTD) method was established, in which the photocathode structure is the same as the material composition and architecture of existing third-generation t-mode NEA GaAs photocathodes. The relationship between structural parameters of the nanopillar array and the 800–900 nm absorption of the photocathode was investigated. By adjusting these parameters, significant absorption enhancement was achieved. Additionally, the effects of film thickness and grating filling material on optical absorption were analyzed. These theoretical analyses that could be verified by the other applicable fields serve as the most important guidance for material selection and structural design of grating-type cathode windows for third-generation image intensifiers.

2. Materials and Methods

The unit cell of the designed "sandwich" nanostructured GaAs photocathode is shown in Figure 1a. The device is mainly comprised of a grating-type cathode glass window and a t-mode GaAs photocathode. The grating-type cathode glass window consists of an anti-

halo photoelectric glass substrate, a SiO_2 layer, a hexagonal close-packed Si_3N_4 nanopillar array with its fill layer, and thin SiO_2 nano-layers. The GaAs photocathode stack includes a SiO_2/Si_3N_4 passivation layer, an $Al_{0.7}Ga_{0.3}As$ window layer, an $Al_{0.2}Ga_{0.8}As$ window layer, and the GaAs emitting layer. The nanopillar array is characterized with period P, pillar diameter D, and pillar height H. Compared with approaches that directly nanostructure the photocathode itself, it is unnecessary for the present design to consider the negative feedback of electron collection efficiency on quantum efficiency [15,19]. Without altering the structure of the GaAs photocathode, the photocathode optical absorption can be controlled by adjusting the structural parameters of the nanopillar array.

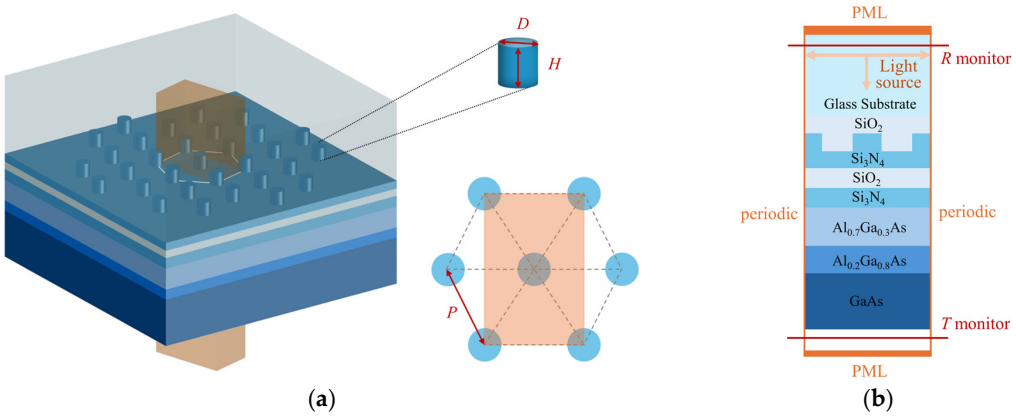


Figure 1. Construction of structural model for "sandwich" nanostructured GaAs photocathode. (**a**) Structural unit of GaAs photocathode inserted into "sandwich" nanostructured layer; (**b**) FDTD simulation region and monitor settings.

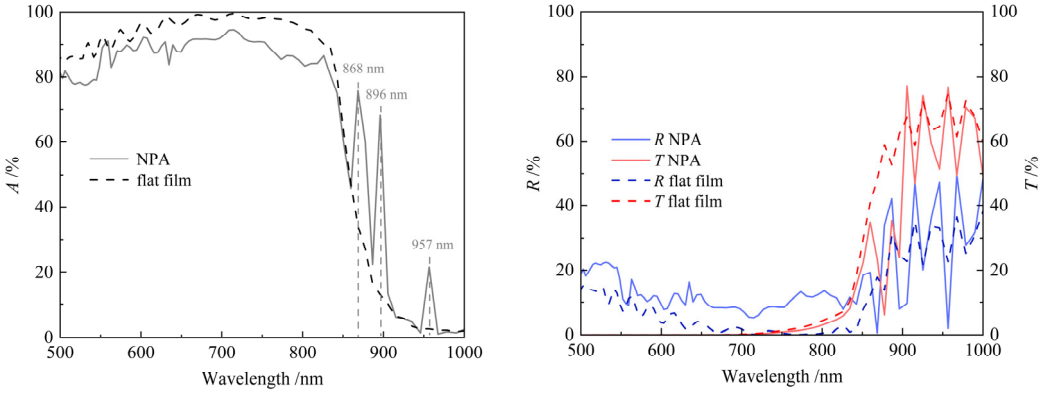
Optical modeling and simulations of the GaAs photocathode were conducted based on the finite-difference time-domain (FDTD) method. The simulation region and monitor arrangement are illustrated in Figure 1b. The horizontal boundary conditions of the simulation region were set to periodic, and the vertical boundary conditions were set to a perfectly matched layer (PML). The light source was a normally incident plane wave with a wavelength range of 500–1000 nm. The reflection (R) and transmission (T) were monitored by placing two-dimensional power monitors on the x–y plane in the SiO_2 window and vacuum, respectively. The reflection monitor (R monitor) was placed above the light source, and the transmission monitor (T monitor) was placed below the emission layer. The absorption (A) was calculated by $A = 1 - R - T$. The refractive indices and extinction coefficients for materials such as Si_3N_4 and GaAs were taken from references [20–27]. For the Si_3N_4 material, the main fitting parameters include fit tolerance 0.03 and max coefficient 6. The simulation mesh was set with mesh accuracy 3, and the nanopillar array region was subjected to mesh refinement, with a step size of 5 nm in the x, y, and z directions; i.e., $dx = dy = dz = 5$ nm.

3. Results and Discussion

3.1. Optimization of Nanopillar Array Structure

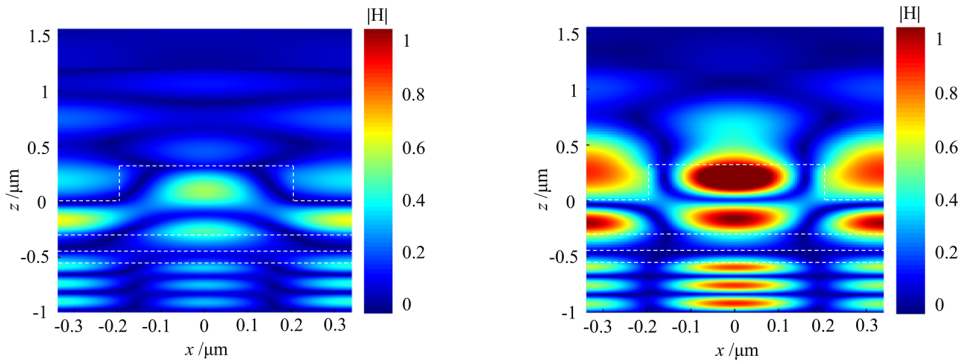
Focusing on achieving high absorption in the near-infrared short-wave range for the GaAs photocathode, the structure of the nanopillar array was firstly optimized. A parameter sweep of the Si_3N_4 nanopillar array structure was performed with a scanning interval of 10 nm, and the optimal structural parameters were determined as P = 680 nm, D = 400 nm, and H = 310 nm. The optical performance of the photocathode with this optimized structure is shown in Figure 2. In comparison with the typical flat film GaAs photocathodes used in third-generation image intensifiers, the nanopillar array photocathode exhibits

a significant enhancement in absorption within the near-infrared band. In particular, at wavelengths of 868 nm, 896 nm, and 957 nm, the absorption is increased by 41.69%, 55.08%, and 18.86%, respectively. Correspondingly, Figure 2b shows that the reflection at these wavelengths decreases substantially, while the transmission increases to varying degrees. Since the wavelength λ = 957 nm exceeds the cutoff wavelength of GaAs photocathodes, the enhancement at this wavelength is of limited practical significance and not be discussed further. To investigate the mechanism by which this nanostructure enhances light absorption, the magnetic field intensity distributions at λ = 868 nm and 896 nm were analyzed through the vertical cross-section of the Si_3N_4 nanopillars, as shown in Figure 3. Local magnetic field hot spots are observed to be periodically distributed along the *x*-axis within the Si_3N_4 nanopillars. This distribution matches the characteristic features of guided-mode resonances excited in waveguide gratings [28], indicating that guided-mode resonance is excited in the nanopillar array structure.



(**a**) (**b**)

Figure 2. Optical properties of Si_3N_4 nanopillar array (NPA) and flat film structured GaAs photocathode. (**a**) Absorption spectra; (**b**) reflection and transmission spectra.



(**a**) (**b**)

Figure 3. Magnetic field intensity distribution through the vertical cross−section of the Si_3N_4 nanopillar, in which the dashed line is the outline of nanopillar and each film layer. (**a**) λ = 868 nm; (**b**) λ = 896 nm.

When incident light interacts with the grating, multiple diffraction orders are generated. Guided-mode resonance occurs when the wave vector of a diffracted order matches the phase of the guided-mode wave vector, causing lateral propagation along the grating surface (the *x*-*y* plane) and confining the energy within the waveguide layer [29,30]. During propagation, the guided-mode experiences leakage due to the periodic perturbation of the grating. The wave leaking upwards undergoes destructive interference with the reflected wave, and the wave leaking downwards undergoes constructive interference with the

transmitted wave. This results in a decrease in reflection and an increase in transmission. Consequently, the optical energy is efficiently directed toward the transmission side and absorbed by the underlying photocathode layers, thereby enhancing the absorption of the photocathode. In the subwavelength regime, only the zeroth-order diffracted light can propagate to the far field, while higher-order diffracted waves become evanescent. Thus, energy is exchanged solely between the zeroth-order reflection and transmission channels, leading to sharp reflection or transmission peaks at the resonance wavelengths. To further investigate this effect, the extinction coefficient of the absorbing material in the model was adjusted to avoid absorption, enabling observation of the intrinsic reflection and transmission characteristics of the nanostructure. At λ = 868 nm and 896 nm, the refractive index of GaAs is 3.54, and only the extinction coefficient k of GaAs is nonzero. For GaAs, the refractive index n was set to 3.54 and the extinction coefficient k was set to 0. The simulated optical response under these conditions is shown in Figure 4. Transmission and reflection peaks appear at 860 nm and 905 nm, respectively, further confirming the presence of guided-mode resonance. The slight deviation from 868 nm and 896 nm may be attributed to approximations in the material refractive index and extinction coefficient.

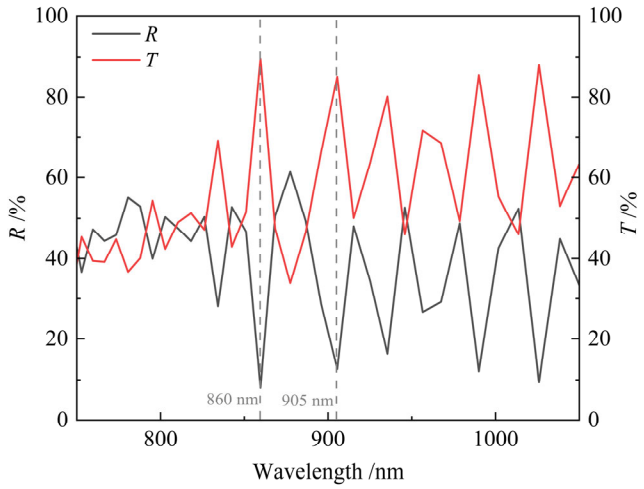


Figure 4. Reflection and transmission spectra of nanopillar array photocathode at n_{GaAs} = 3.54 and k_{GaAs} = 0.

3.2. Influence of Varied Nanopillar Array Structure on Photocathode Absorption

During the fabrication of nanostructures, the structural parameters generally show a gap from the theoretical design due to inevitable errors introduced by lithography and etching. To determine the acceptable tolerance range, the effects of each structural parameter of the nanopillar array on the photocathode absorption were investigated based on the modelling optimized structure. Figure 5 shows the absorption spectra of photocathodes with different array periods. As the nanopillar period increases, the number, position, and peak values of the absorption peaks all change. Specifically, at λ = 868 nm and 896 nm, the peak absorption first increases and then decreases as the period increases, with a large amplitude of change. Existing studies on the influence of waveguide structural parameters on guided-mode resonance mainly focus on single-layer or double-layer waveguide grating structures. However, the nanostructured photocathode model in this work is a multilayer waveguide grating structure. The influence of the nanostructure parameters on photocathode absorption differs from the trends predicted by the conventional guided-mode resonance theory. This difference could be attributed to the mutual influence between guided-mode resonance and effects such as thin-film interference. The effects of nanopillar diameter and height on the photocathode absorption are shown in Figure 6, and they exhibit similar trends. Taking diameter as an example, the peak absorption at λ = 868 nm and 896 nm

first increases and then decreases as the diameter increases. At λ = 868 nm, the peak varies slowly with diameter, resulting in a wider bandwidth for the peak absorption–diameter curve. At λ = 896 nm, the variation is faster and the curve is narrower.

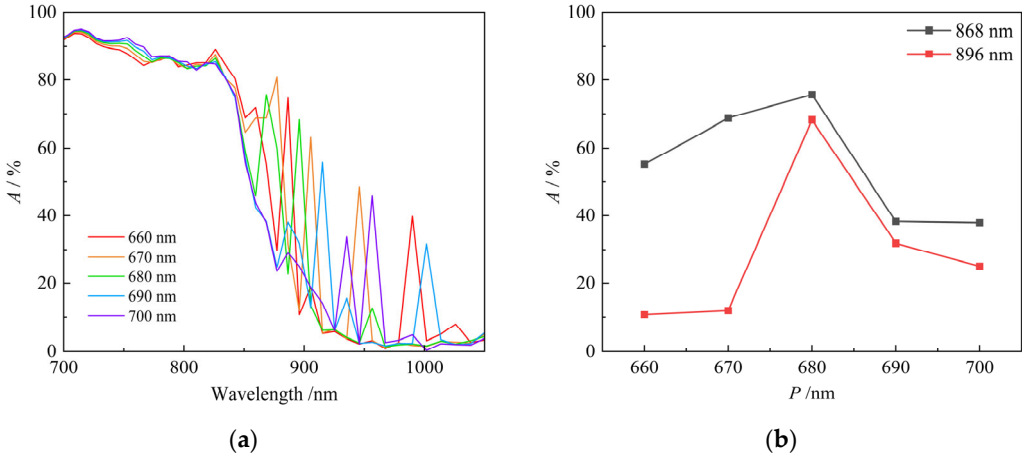


Figure 5. The relationship between the period of nanopillar array and the light absorption of the photocathode. (**a**) Photocathode absorption spectra at different periods; (**b**) variation in peak absorption with period at λ = 868 nm and 896 nm.

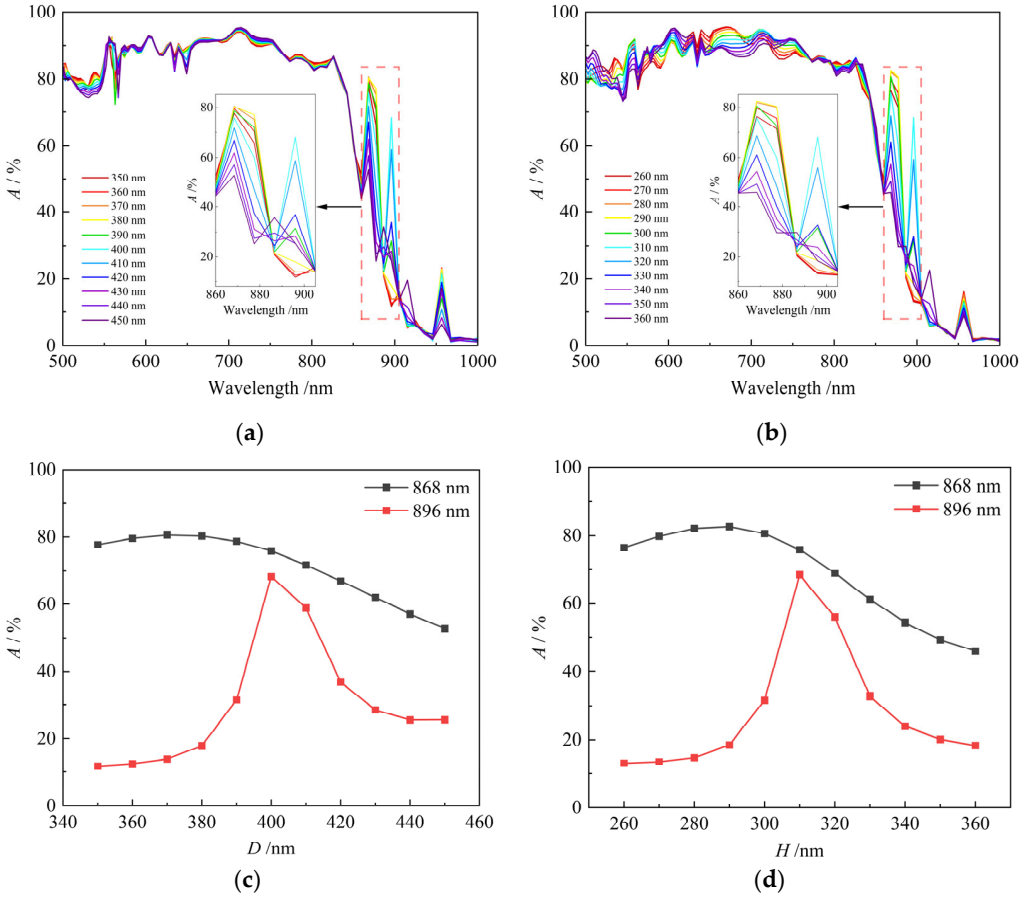


Figure 6. The relationship between the structural parameters and the light absorption of the photocathode. (**a**) Photocathode absorption spectra at different nanopillar diameters; (**b**) photocathode absorption spectra at different nanopillar heights; (**c**,**d**) variation in peak absorption with diameter and height at λ = 868 nm and λ = 896 nm.

3.3. Influence of Refractive Index of the Grating Filling Material on Photocathode Absorption

Keeping the structural parameters unchanged, the effect of the filling material's refractive index on the photocathode absorption was investigated. The filling material Si_3N_4 (n ~ 2.06) was modified to other dielectrics including Al_2O_3 (n ~ 1.68), HfO_2 (n ~ 1.89), Ta_2O_5 (n ~ 2.13), and TiO_2 (n ~ 2.5), and the comparative results are shown in Figure 7. The refractive index has a significant regulatory effect on the photocathode's light absorption, with clear performance differences among the various grating filling materials. In the visible light band and parts of the near-infrared short-wave region ($\lambda < 850$ nm), the absorption of the grating photocathodes with all filling materials is lower than that of the flat film photocathode. When λ is over 850 nm, however, the grating structure photocathodes in all groups exhibit several absorption peaks, showing a distinct enhancement compared to the flat film photocathode. Furthermore, the peak positions and values of the absorption peaks vary among the different filling materials. According to the optical absorptivity in the near-infrared short-wave region and considering the cut-off wavelength of the GaAs photocathode, the integral absorptivity of the photocathode in the 850–950 nm band under different filling materials is calculated (Table 1), and it is concluded that Si_3N_4 is the best grating filling material for optical absorption enhancement.

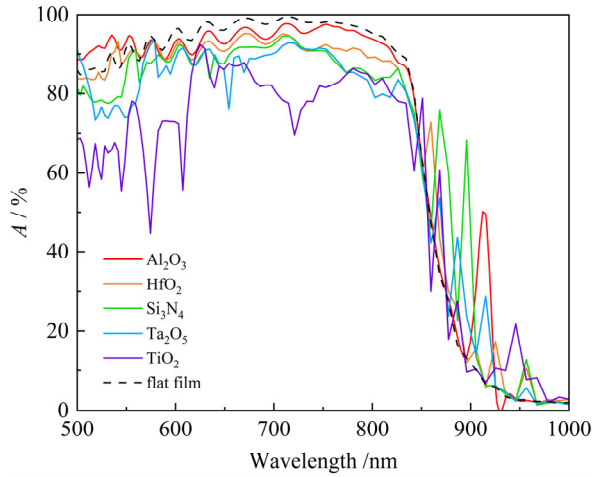


Figure 7. Influence of grating filling materials on light absorption of photocathode.

Table 1. Integrated absorptivity of photocathodes in 850–950 nm band with different grating filling materials.

Material	Integrated Absorptivity in 850–950 nm Band
Al_2O_3	25.35%
HfO_2	24.09%
Si_3N_4	31.18%
Ta_2O_5	25.68%
TiO_2	22.97%
Flat film	18.54%

3.4. Influence of SiO_2 Thickness on Photocathode Absorption

Considering the requirements of practical fabrication processes, in order to prevent the Si_3N_4 from being damaged during the bonding of the photocathode optical window with the GaAs epitaxial wafer, a SiO_2 thin film is deposited on the surface of Si_3N_4 filling material. This allows the bonding process to occur between two SiO_2 surfaces, improving material compatibility and process adaptability. Therefore, the influence of the SiO_2 film thickness (d_1) on the optical absorption was investigated, and the results are shown in Figure 8. As the film thickness increases, the absorption peak at λ = 868 nm decreases, while

the peak at λ = 896 nm first increases and then decreases. Based on the simulation results, the integrated absorption in the near-infrared region indicates that the system achieves the optimum absorption and protection from damage when the SiO_2 film thickness is 180 nm. Since the GaAs epitaxial wafer used in third-generation image intensifiers already contains a native 170 nm thick SiO_2 layer on its surface, a 10 nm thick SiO_2 film can be deposited on the Si_3N_4 during grating fabrication. This configuration not only achieves the optimal optical absorption but also protects the Si_3N_4 filling material from structural damage during the bonding process.

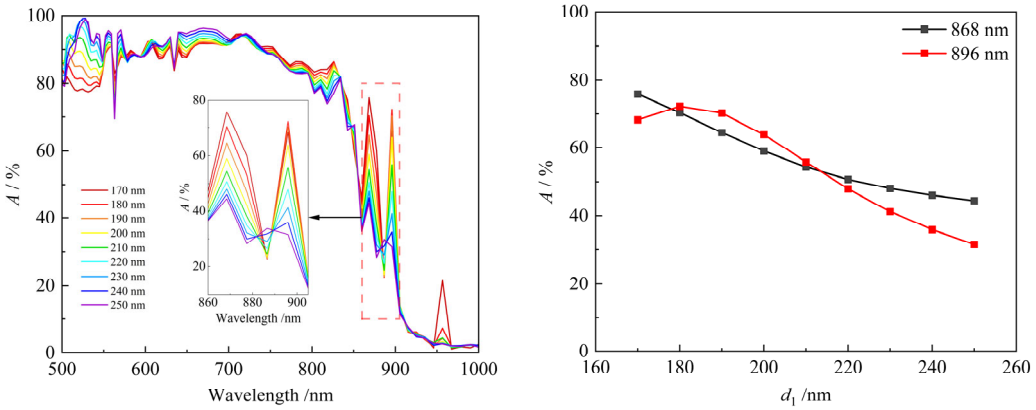


Figure 8. The relationship between the thickness of SiO_2 layer and the absorption spectrum of photocathode. (**a**) The absorption spectra of photocathode with different d_1; (**b**) variation in peak absorption with d_1 at λ = 868 nm and λ = 896 nm.

3.5. Discussion

This design focuses on the GaAs photocathode used in third-generation image intensifiers. Without altering the original photocathode structure, enhanced optical absorption in specific wavelength bands is achieved. Meanwhile, micro-nano fabrication processes are taken into consideration, and corresponding investigations and optimizations are conducted to facilitate practical fabrication and production. At present, the commonly adopted approach for nanostructured NEA GaAs photocathodes is to directly pattern the photocathode surface. Taking a Mie-type nanopillar array reflective GaAs photocathode [15] as an example, the generated photoelectrons are highly localized inside the nanopillars, mainly near the top surfaces and sidewalls. However, not all of these photoelectrons can be effectively transported and emitted into the vacuum. In the absence of space-charge effects and external electromagnetic fields, only electrons emitted within a limited angular range can be collected and thus contribute positively to the quantum efficiency. Electrons emitted outside this angular range are likely to be trapped by the nanopillar sidewalls (e.g., laterally emitted electrons), which leads to a negative impact on the QE. In contrast, the proposed design preserves the planar structure of the GaAs photocathode. As a result, issues related to electron collection efficiency and its negative feedback on the quantum efficiency do not need to be considered.

4. Conclusions

This study proposes a nanostructured t-mode GaAs NEA photocathode in which a Si_3N_4 nanopillar array grating is employed to enhance optical absorption while preserving the original photocathode structure and thereby improve photoemission performance. By reproducing the composition and configuration of the t-mode GaAs NEA photocathodes used in existing third-generation image intensifiers, the optimized structural parameters of nanopillar array as P = 680 nm, D = 400 nm, and H = 310 nm for the modelled photocathode

structure are achieved. The significant absorption enhancement in the near-infrared region, especially at characteristic wavelengths of 868 nm and 896 nm, are realized, showing the absorption increases by 41.69% and 55.08% in comparison with a typical flat film GaAs photocathode. Fully considering the micro-nano fabrication processes in practice, the structural parameters including the period, diameter, and height of the nanopillar array are adjusted to investigate the influence on optical absorption. It is shown that the period should be focused on more in controlling the optimum value. According to the comparison with the other grating filling materials, Si_3N_4 is indeed the most effective filling material for enhancing near-infrared absorption with the designed structure parameters due to the suitable refractive index. During grating fabrication with Si_3N_4 as the filling material, a 10 nm SiO_2 layer may be deposited on the Si_3N_4 surface to protect the Si_3N_4 from structural damage during the bonding process without negatively impacting the light absorption performance. In future work, grating-type cathode optical window samples will be fabricated according to the optimized parameters and bonded to GaAs photocathodes.

Author Contributions: Conceptualization, J.Y. and Y.H. (Yonggang Huang); methodology, Z.X.; formal analysis, M.D.; writing—original draft, Z.X.; writing—review and editing, Y.H. (Yonggang Huang) and Y.X.; supervision, P.S., Y.H. (Ying He) and J.C.; project administration, P.J. and Y.D.; funding acquisition, Y.H. (Yonggang Huang). All authors have read and agreed to the published version of the manuscript.

Funding: This work is supported by the National Natural Science Foundation of China (No. 52072357), the Young Elite Scientists Sponsorship Program by CAST, the Youth Talent Support Project of Beijing Association for Science and Technology (No.BYESS2024388), the Major Scientific and Technological Research Projects in the National Building Materials Industry of the China Building Materials Federation (No.202201JBGS11-01), and the Key Core Technology Research Projects of China National Building Materials Group (No.2023SJYL07).

Institutional Review Board Statement: Not applicable.

Informed Consent Statement: Not applicable.

Data Availability Statement: Data underlying the results presented in this paper are not publicly available at this time but may be obtained from the authors upon reasonable request.

Conflicts of Interest: Author Ziyang Xiao, Miao Dong, Yonggang Huang, Jinhui Yang, Peng Jiao, Pan Shi, Yajie Du, Jing Cheng were employed by the company China Building Materials Academy. Author Pan Shi was also were employed by the company China National Building Material Guangxin Technology Co., Ltd. The remaining authors declare that the research was conducted in the absence of any commercial or financial relationships that could be construed as a potential conflict of interest.

References

1. Zhao, J.; Yu, H.; Liu, W.; Guo, J. Analysis of the Relation between Spectral Response and Absorptivity of GaAs Photocathode. *Acta Phys. Sin.* **2017**, *66*, 227801. [CrossRef]
2. Chen, X.; Tang, G.; Wang, D.; Xu, P. High Quantum Efficiency Transmission-Mode GaAlAs Photocathode with a Nanoscale Surface Structure. *Opt. Mater. Express* **2018**, *8*, 3155. [CrossRef]
3. Zhang, Y. Progress in Research on Semiconductor Photocathodes. *Infrared Technol.* **2022**, *44*, 778–791.
4. Cai, Z.; Huang, W.; Yang, C.; Lou, B.; He, J. Theoretical Study of the Average Decay Time and Response Characteristics of the Transmission-Mode GaAs Photocathodes with the Different Doping Gradient Distribution. *Chin. J. Vac. Sci. Technol.* **2025**, *45*, 398–407. [CrossRef]
5. Xie, H. Overview of the Semiconductor Photocathode Research in China. *Micromachines* **2021**, *12*, 1376. [CrossRef]
6. Zhang, Q.; Bai, X.; Cheng, H.; Jiao, G.; Li, Z.; Han, K.; Li, Q. Research on Signal-to-noise Ratio of Low-light Level Image Intensifier Based on Night Sky Light Spectrum Matching. *Acta Phys. Sin.* **2022**, *51*, 0304005. [CrossRef]
7. Spicer, W.E. Photoemissive, Photoconductive, and Optical Absorption Studies of Alkali-Antimony Compounds. *Phys. Rev.* **1958**, *112*, 114–122. [CrossRef]

8. Zhang, Y.; Chang, B.; Niu, J.; Zhao, J.; Zou, J.; Shi, F.; Cheng, H. High-Efficiency Graded Band-Gap $Al_xGa_{1-x}As$/GaAs Photocathodes Grown by Metalorganic Chemical Vapor Deposition. *Appl. Phys. Lett.* **2011**, *99*, 101104. [CrossRef]
9. Zhang, Y.; Niu, J.; Zhao, J.; Zou, J.; Chang, B.; Shi, F.; Cheng, H. Influence of Exponential-Doping Structure on Photoemission Capability of Transmission-Mode GaAs Photocathodes. *J. Appl. Phys.* **2010**, *108*, 093108. [CrossRef]
10. Feng, C.; Zhang, Y.; Liu, J.; Qian, Y.; Liu, X.; Shi, F.; Cheng, H. Effect of Graded Bandgap Structure on Photoelectric Performance of Transmission-Mode $Al_xGa_{1-x}As$/GaAs Photocathode Modules. *Appl. Opt.* **2017**, *56*, 9044–9049. [CrossRef]
11. Feng, C.; Zhang, Y.; Qian, Y.; Xu, Y.; Liu, X.; Jiao, G. Quantum Efficiency of Transmission-Mode $Al_xGa_{1-x}As$/GaAs Photocathodes with Graded-Composition and Exponential-Doping Structure. *Opt. Commun.* **2016**, *369*, 50–55. [CrossRef]
12. Wang, D.; Zhang, Y.; Li, S.; Tong, Z.; Tang, S.; Shi, F.; Jiao, G.; Cheng, H.; Fu, R.; Qian, Y.; et al. AlGaAs Photocathode with Enhanced Response at 532 nm. *Acta Phys. Sin.* **2024**, *73*, 118503. [CrossRef]
13. Nützel, G.; Lavoute, P. Semi-Transparent Photocathode with Improved Absorption Rate. U.S. Patent US20150279606A1, 1 May 2018.
14. Peng, X.; Wang, Z.; Liu, Y.; Manos, D.M.; Poelker, M.; Stutzman, M.; Tang, B.; Zhang, S.; Zou, J. Optical-Resonance-Enhanced Photoemission from Nanostructured GaAs Photocathodes. *Phys. Rev. Appl.* **2019**, *12*, 064002. [CrossRef]
15. Peng, X.; Poelker, M.; Stutzman, M.; Tang, B.; Zhang, S.; Zou, J. Mie-Type GaAs Nanopillar Array Resonators for Negative Electron Affinity Photocathodes. *Opt. Express* **2020**, *28*, 860. [CrossRef]
16. Li, S.; Zhang, Y.; Wang, Z.; Wang, D.; Tang, S.; Zhang, J.; Shi, F.; Jiao, G.; Cheng, H.; Hao, G. Enhanced Blue-Green Response of Nanoarray AlGaAs Photocathodes for Underwater Low-Light Detection. *Opt. Express* **2023**, *31*, 26014–26026. [CrossRef] [PubMed]
17. Li, S.; Zhang, Y.; Tang, S.; Yang, L.; Ma, X.; Gao, J.; Tong, Z.; Qian, Y.; Shi, F.; Guo, X. Near-Infrared Enhancement in Thin Transmission-Mode GaAs Photocathodes via Nanostructured Window Layer. *Opt. Express* **2025**, *33*, 38543–38552. [CrossRef]
18. Peng, X.; Zhong, C.; Zou, J.; Deng, W. All-Dielectric Meta-Surface Transmission-Mode Ultra-Thin GaAs Negative Electron Affinity Photocathode. *Appl. Phys. Lett.* **2024**, *125*, 071103. [CrossRef]
19. Dong, M.; Wang, L.; Chen, D.; Kang, G.; Gong, Y.; Wang, Y.; Zheng, D.; Zhao, Y.; Cai, Y. Absorption-Enhanced Nanopillar-Arrayed Na_2KSb Photocathode for Improving Image Intensifier Performance. *Opt. Express* **2025**, *33*, 36025–36036. [CrossRef]
20. Malitson, I.H. Interspecimen Comparison of the Refractive Index of Fused Silica. *J. Opt. Soc. Am.* **1965**, *55*, 1205–1208. [CrossRef]
21. Luke, K.; Okawachi, Y.; Lamont, M.R.E.; Gaeta, A.L.; Lipson, M. Broadband Mid-Infrared Frequency Comb Generation in a Si_3N_4 Microresonator. *Opt. Lett.* **2015**, *40*, 4823–4826. [CrossRef]
22. Aspnes, D.E.; Kelso, S.M.; Logan, R.A.; Bhat, R. Optical Properties of $Al_xGa_{1-x}As$. *J. Appl. Phys.* **1986**, *60*, 754–767. [CrossRef]
23. Papatryfonos, K.; Angelova, T.; Brimont, A.; Reid, B.; Guldin, S.; Smith, P.R.; Tang, M.; Li, K.; Seeds, A.J.; Liu, H.; et al. Refractive Indices of MBE-Grown $Al_xGa_{(1-x)}As$ Ternary Alloys in the Transparent Wavelength Region. *AIP Adv.* **2021**, *11*, 025327. [CrossRef]
24. Bright, T.J.; Watjen, J.I.; Zhang, Z.M.; Muratore, C.; Voevodin, A.A.; Koukis, D.I.; Tanner, D.B.; Arenas, D.J. Infrared Optical Properties of Amorphous and Nanocrystalline Ta_2O_5 Thin Films. *J. Appl. Phys.* **2013**, *114*, 083515. [CrossRef]
25. Boidin, R.; Halenkovič, T.; Nazabal, V.; Beneš, L.; Němec, P. Pulsed Laser Deposited Alumina Thin Films. *Ceram. Int.* **2016**, *42*, 1177–1182. [CrossRef]
26. Al-Kuhaili, M.F. Optical Properties of Hafnium Oxide Thin Films and Their Application in Energy-Efficient Windows. *Opt. Mater.* **2004**, *27*, 383–387. [CrossRef]
27. Siefke, T.; Kroker, S.; Pfeiffer, K.; Puffky, O.; Dietrich, K.; Franta, D.; Ohlídal, I.; Szeghalmi, A.; Kley, E.; Tünnermann, A. Materials Pushing the Application Limits of Wire Grid Polarizers Further into the Deep Ultraviolet Spectral Range. *Adv. Opt. Mater.* **2016**, *4*, 1780–1786. [CrossRef]
28. Magnusson, R.; Ko, Y.H. Guided-Mode Resonance Device Technology: Design, Fabrication, Applications and Prospects. In Proceedings of the 2017 Photonics North (PN), Ottawa, ON, Canada, 6–8 June 2017; p. 1. [CrossRef]
29. Khaleque, T.; Magnusson, R. Light Management through Guided-Mode Resonances in Thin-Film Silicon Solar Cells. *J. NanoPhotonics* **2014**, *8*, 083995. [CrossRef]
30. Fallah, H.; Hakim, L.; Boonruang, S.; Mohammed, W.S.; Hsu, S.H. Polymer-Based Guided-Mode Resonance Sensors: From Optical Theories to Sensing Applications. *ACS Appl. Polym. Mater.* **2023**, *5*, 9700–9713. [CrossRef]

Disclaimer/Publisher's Note: The statements, opinions and data contained in all publications are solely those of the individual author(s) and contributor(s) and not of MDPI and/or the editor(s). MDPI and/or the editor(s) disclaim responsibility for any injury to people or property resulting from any ideas, methods, instructions or products referred to in the content.